

pubs.acs.org/acscatalysis Research Article

# Design of Dilute Palladium-Indium Alloy Catalysts for the Selective Hydrogenation of CO<sub>2</sub> to Methanol

Abdulaziz M. Alamer, Mengyao Ouyang, Faisal H. Alshafei, Muhammad Amtiaz Nadeem, Yahya Alsalik, Jeffrey T. Miller, Maria Flytzani-Stephanopoulos, E. Charles H. Sykes, Vasilios Manousiouthakis, and Nathaniel M. Eagan\*



Cite This: ACS Catal. 2023, 13, 9987-9996



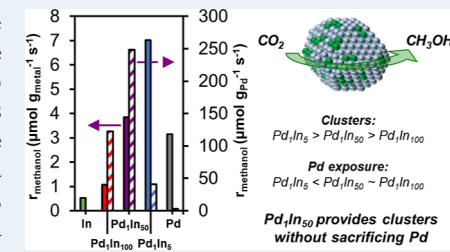
**ACCESS** 

III Metrics & More

Article Recommendations

Supporting Information

ABSTRACT: Adding small amounts of a more reactive dopant metal to a more selective host metal is a well-known strategy for promoting the catalytic reactivity of the latter without sacrificing its selectivity. While substantial attention has been given to coinage metal hosts for activating individual C-H or O-H bonds, less attention has been given to more exotic metals, such as indium, which is highly selective in the complex hydrogenation of CO2 to methanol. Herein, we describe the synthesis and properties of Pd-In alloys containing Pd in various states of aggregation (isolated atom, small clusters, and extended clusters) assessed through various characterization methods. These materials exhibit unique catalytic behaviors, with Pd promoting both



the reaction rate and methanol selectivity in all cases, though its efficacy is highest when Pd is present in small clusters. The inefficiency of high Pd loadings is due in part to losses in Pd accessibility, while the importance of aggregated vs isolated Pd is theorized to result from accelerated H<sub>2</sub> activation. Methods used to synthesize more conventional dilute-limit and single-atom alloy catalysts can, therefore, be extended to non-coinage metal hosts to promote and control more complex chemistries, though the roles of ensemble size may greatly differ.

KEYWORDS: carbon dioxide, indium, alloys, methanol, galvanic replacement

# 1. INTRODUCTION

Carbon dioxide (CO<sub>2</sub>) is a major air pollutant and a potent greenhouse gas emitted from a wide range of human activities including transportation, electricity generation, and industry. In the past few decades, a dramatic increase in the earth's atmospheric CO<sub>2</sub> concentration (to >400 ppm) has led to concerns regarding global climate changes with possibly irreversible environmental ramifications. 1,2 Catalytic conversion of CO<sub>2</sub> into value-added chemicals is an attractive route for mitigation<sup>5</sup> as it provides a clear economic incentive for harvesting CO<sub>2</sub> rather than emitting it. The conversion of CO<sub>2</sub> into methanol<sup>4</sup> has been at the nexus of these utilization efforts due to the fact that methanol already serves as a key building block in the chemical industry for the production of methyl tert-butyl ether, acetic acid, formaldehyde, and dimethyl ether, prompting calls for the establishment of a "methanol economy."10

Although methanol is commercially synthesized from syngas (CO/CO<sub>2</sub>/H<sub>2</sub> mixtures) using a Cu/ZnO/Al<sub>2</sub>O<sub>3</sub> catalyst, <sup>1</sup> this material has a low tolerance for high CO<sub>2</sub> concentrations, which leads to deactivation via sintering. 12 In the search for novel catalysts for methanol synthesis from CO2, density functional theory calculations have identified indium oxide  $(In_2O_3)^{13,14}$  as a promising catalytic material due to its ability to promote CO2 conversion through a selective formate pathway without aiding the parasitic water-gas shift reaction.

Subsequent experimental tests of ZrO<sub>2</sub>-supported In<sub>2</sub>O<sub>3</sub> displayed total methanol selectivity and stability for over 1000 h under industrially relevant conditions (T = 573 K, P =5.0 MPa,  $H_2/CO_2 = 4$ , GHSV = 16,000 h<sup>-1</sup>). Nonetheless, indium has an inherently limited ability to activate molecular hydrogen; hence, a second metal that can more readily promote this step such as Pd16,17 or Pt18,19 is required to enhance the material's catalytic activity toward CO2 conversion.

Due to the scarcity and high cost of noble metal promoters such as Pd and Pt, it is of great importance to design catalysts that expose as much of the noble metal to the reactant stream as possible while maintaining their catalytically active configurations under reaction conditions. This has been achieved at the extreme limit with the promoter fully dispersed either on a support (single-atom catalyst)<sup>20,21</sup> or within another host metal (single-atom alloy). 22,23 While many promising reports of the catalytic activities of these materials

Received: April 25, 2023 Revised: June 22, 2023 Published: July 17, 2023





exist, there are various chemistries that they commonly cannot facilitate (e.g., C–C bond cleavages). <sup>2,4–2,8</sup> In such cases, nanoclusters of the noble metals may instead be required.

Recently, Pérez-Ramirez and co-workers highlighted the promotional role Pd can play when anchored to bulk In<sub>2</sub>O<sub>3</sub>, noting that small clusters of Pd (2-3 atoms) were key to improving the rate, selectivity, and stability of methanol synthesis from CO<sub>2</sub>. <sup>17</sup> While the addition of isolated Pd atoms increased the reaction rate and selectivity to methanol, clusters in the two- to three-atom range were more effective due to their improved H2 dissociation capabilities. Synthesis of these clusters required the use of low Pd loadings to ensure that Pd was primarily anchored to the In<sub>2</sub>O<sub>3</sub> rather than to other Pd atoms. Larger Pd clusters (>4) behaved more like extended Pd and promoted the parasitic reverse water-gas shift reaction, which undesirably converts CO<sub>2</sub> into CO instead of methanol. Pérez-Ramirez and co-workers also noted that the choice of synthesis method was important, with co-precipitation generally producing more uniform and stable catalytic materials than dry impregnation. Tunability of this system is somewhat limited, however, as the support identity (In<sub>2</sub>O<sub>3</sub>) is critical and thus cannot be varied, while the selectivity and stability are highly sensitive to Pd loading.

Herein, we investigate the promotional effects of dilute Pd in metal-in-metal Pd-In alloys rather than in metal-on-metal oxide Pd/In<sub>2</sub>O<sub>3</sub> in order to decouple the active phase from the support and expand opportunities for selective CO<sub>2</sub> hydrogenation. We demonstrate a new synthesis approach for Inbased CO<sub>2</sub> hydrogenation catalysts, whereby the galvanic replacement (GR) method is used to controllably exchange Pd into In nanoparticles anchored to a conventional metal oxide support  $(\gamma-Al_2O_3)$ , which only serves to disperse the In nanoparticles. Prior studies have shown GR to be effective for synthesizing dilute alloys with controllable composition while mitigating the deposition of the promoter metal onto the support, <sup>29</sup>-33 but to the best of our knowledge, this has not yet been demonstrated with In-based systems. We hypothesized that this colocation of Pd and In would be important for controlling CO2 hydrogenation selectivity since it has been previously shown that the CO formation rate in methanol steam reforming over Pd is greatly diminished when alloying with In.<sup>34</sup> Here, the structural and catalytic behaviors of Pd in GR-synthesized Pd-In alloys were interrogated, and our results reveal that distinct Pd structures can be produced by varying the alloy composition and exploited to obtain favorable catalytic performance. The Pd-In alloy catalysts showed unique reactivities with the alloy containing small aggregates of Pd, exhibiting a substantial improvement in methanol production rate and selectivity relative to isolated Pd atoms.

## 2. EXPERIMENTAL SECTION

**2.1.** Synthesis of Pd–In Alloy Catalysts via Galvanic Replacement.  $In_2O_3$  supported on gamma alumina,  $\gamma$ -Al $_2O_3$  (Inframat, 99.995%), was synthesized via incipient wetness impregnation (IWI) where a desired amount of indium(III) nitrate hydrate,  $In(NO_3)_3$ : $xH_2O$  (Aldrich, 99.9%), was dissolved in deionized water (DI) and then impregnated on  $\gamma$ -Al $_2O_3$  ( $\sim$ 1.08 mL  $g_{\gamma$ -Al $_2O_3$ <sup>-1</sup>). The as-synthesized catalyst was then thermally treated in air at 300 °C (5 °C min<sup>-1</sup> ramp) for 3 h and then reduced at 350 °C (10 °C min<sup>-1</sup> ramp) under 5%  $H_2$  in Ar (20 mL min<sup>-1</sup>) for 2 h. Separately, 150 mL of DIwater was brought to a boil in an Ar environment. Sodium

borohydride, NaBH<sub>4</sub> (Aldrich, 99%), was added dropwise to the water to reach a concentration of 0.1 M and stirred for 15 min. The reduced In/Al<sub>2</sub>O<sub>3</sub> was added to the boiled DI water without exposure to air. To further prevent the oxidation of the supported In, 0.1 M ascorbic acid (Aldrich, 99%) was added to the solution after 15 min of stirring. The subsequent addition of Pd atoms exclusively to In nanoparticles was then achieved via galvanic replacement ( $\Delta E^{\circ} = 1.28$  V) where the Pd precursor is favorably reduced by the In host metal according to the following two half-reactions

$$Pd^{2+} + 2e^{-} \rightarrow Pd^{0} \quad \Delta E^{\circ} = 0.951 \text{ V}$$
  
 $In^{0} \rightarrow In^{3+} + 3e^{-} \quad \Delta E^{\circ} = 0.338 \text{ V}$ 

To achieve this, a desired amount of palladium(II) nitrate hydrate,  $Pd(NO_3)_2 \cdot xH_2O$  (Aldrich), was dissolved in DI  $H_2O$  and then added to the solution while stirring. The resulting material was filtered and washed with 1 L of DI  $H_2O$ . The acquired powder was then dried overnight under vacuum at 120 °C.

2.2. Materials Characterization. Inductively coupled plasma atomic emission spectroscopy (ICP-AES) measurements were conducted on a Leeman Labs PS1000 instrument. The catalyst samples were digested in 2 mL of an aqua regia solution overnight and then further diluted in DI-H<sub>2</sub>O to obtain the desired concentration (typically 1–100 ppm) of the metal. X-ray diffraction (XRD) was performed on a Rigaku instrument. Cu K $\alpha$  radiation was used with a power setting of 30 mA and 15 kV. Data were collected from 10 and 70°  $2\theta$ with a step size of 0.01° and a scan speed of 0.15° min<sup>-1</sup>. X-ray photoelectron spectroscopy (XPS) spectra were obtained on a Kratos Axis Ultra DLD system equipped with a monochromatic Al K\alpha X-ray source and a double focusing hemispherical analyzer. For all samples, 40 scans were collected for the Pd 3d region and 20 scans for the In 3d region, and the XPS data were analyzed using the Thermo Avantage software. The reduced fresh catalysts were exposed to air for  $\sim 1-2$  min during sample loading. Electron microscopy studies were performed using a Titan ST microscope (FEI Company) operated at an accelerating voltage of 300 kV. The microscope was operated either in TEM-mode (phase contrast) or highangle annular dark field (HAADF)-STEM mode (Z-contrast). The TEM beam focus was 100 nm, while that of STEM was 1.0 nm. Energy-dispersive X-ray spectroscopy (EDS) analyses were performed on catalysts with exposed areas smaller than or equal to the image size to facilitate the microscopic analysis when EDS was conducted in the TEM mode of operation. For each sample, approximately 50 EDS spectra were collected, and two representative spectra for each catalyst are shown in the Supporting Information section.

Diffuse reflectance infrared Fourier transform spectroscopy (DRIFTS) measurements were performed on a Thermo Scientific Nicolet iS50 FTIR spectrometer equipped with a DTGS KBr detector and a Harrick Praying Mantis high-temperature reaction cell (HVC-DRP4) equipped with ZnSe and quartz windows. In a typical experiment, the catalyst sample was purged with He while heating to 300 °C, after which the gas mixture was switched to 10%  $\rm H_2$  in He at a flow rate of 12 mL min<sup>-1</sup> for 1 h. After reduction, the sample was purged with He gas at 300 °C for 10 min and subsequently cooled to room temperature under He with a flow rate of 12 mL min<sup>-1</sup>, after which a background spectrum was recorded. Thereafter, 3% CO in He gas mixture was introduced into the

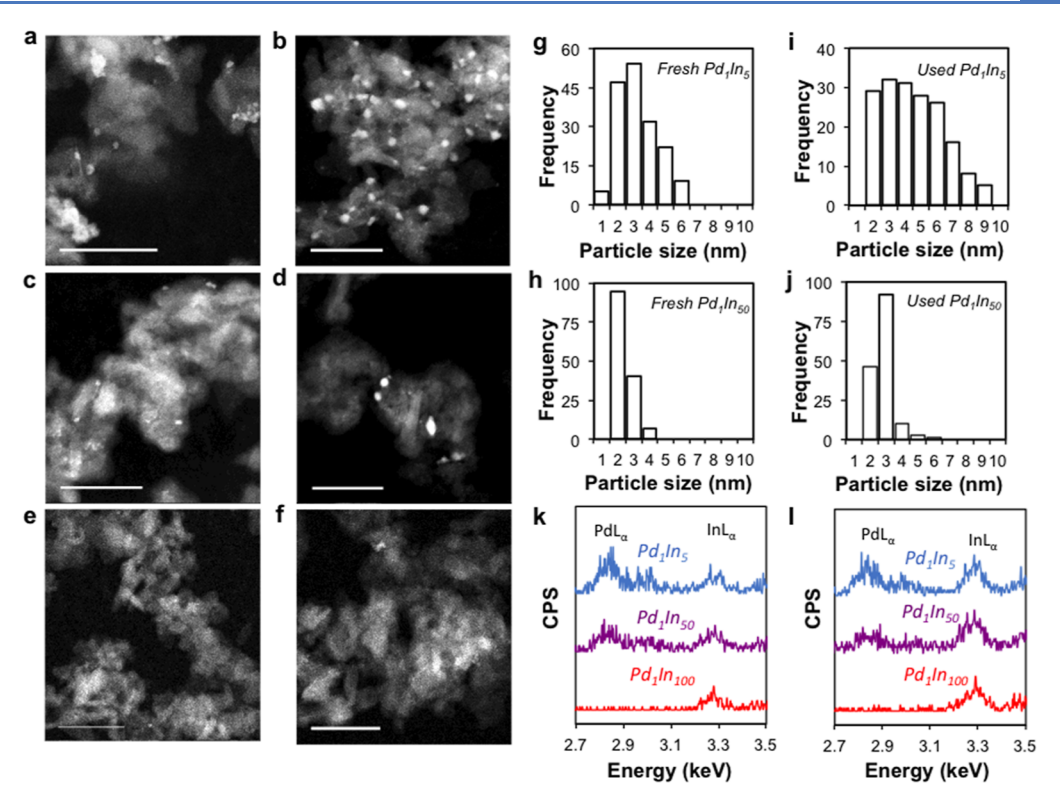


Figure 1. HAADF-STEM images of Pd–In alloys, average particle size distributions, and STEM EDS spectra. (a) Fresh  $Pd_1In_5$  catalyst. (b) Used  $Pd_1In_5$  catalyst. (c) Fresh  $Pd_1In_{50}$  catalyst. (d) Used  $Pd_1In_{50}$  catalyst. (e) Fresh  $Pd_1In_{100}$  catalyst. (f) Used  $Pd_1In_{100}$  catalyst. (g–j) Average particle distribution for Pd–In alloys. (k) STEM-EDS spectra of fresh Pd–In alloys. (l) STEM-EDS spectra of used Pd–In alloys. The scale bar in all images is 50 nm.

cell for 30 min at a flow rate of 12 mL min<sup>-1</sup> during which spectra were collected every 2–5 min. While continuing to collect spectra, the sample cell was then purged with He at a flow rate of 12 mL min<sup>-1</sup> for a minimum of 30 min. Each CO-DRIFTS spectrum was recorded at 25 °C with a spectral resolution of 4 cm<sup>-1</sup> with an average of 96 scans.

X-ray absorption spectroscopy (XAS) measurements were carried out in the 8-ID beamline at the National Synchrotron Light Source II of Brookhaven National Laboratory. The in situ Pd K-edge (24.359 keV) X-ray absorption near-edge spectroscopy (XANES) spectra were collected using the fluorescence mode in a Clausen cell flow reactor under atmospheric pressure. The catalyst (~2 mg) was loaded in a quartz tube (1.0 mm OD and 0.9 mm ID), and 10 mL min<sup>-1</sup> H<sub>2</sub> was introduced into the system. The sample was heated from room temperature to the desired temperature with a 10 °C min<sup>-1</sup> ramping rate. The ex situ extended X-ray absorption fine structure (EXAFS) spectra were collected in the same beamline with samples mounted via Kapton tape. Energy calibration was performed based on the Pd K-edge energy (24.359 keV) of a Pd foil standard. Data processing was performed using the IFEFFIT package. Depending on the Pd loading, 15-35 spectra were averaged. The average spectra were fit using WinXAS software. Phase and amplitude functions were prepared from experimental references: Pd foil (12 Pd-Pd at 2.75 Å) and PdO (4 Pd-O at 2.05 Å). Fitting was initially performed in R space on  $k^2$ -weighted chi, with  $\Delta k = 2.8 - 11.4 \text{ Å}^{-1}$  and  $\Delta R = 1.0 - 2.0 \text{ Å}$  for PdO or  $\Delta R =$ 1.3-2.9 Å for used and reduced samples. Optimized fits were determined in k-space on  $k^2$ -weighted chi of the isolated Pd-O or Pd-M (M = Pd or In) shells to determine the best  $\Delta \sigma^2$ values. The  $\Delta \sigma^2$  values of each sample were similar; therefore,

the average value of all samples was taken and fixed in the final fits.

**2.3. Catalytic Evaluations.** The catalytic performance of the Pd-In catalysts for CO<sub>2</sub> hydrogenation to methanol was evaluated in a fixed bed reactor at a pressure of 30 bar, at temperatures between 240 and 300 °C, and with a gas-hourly space velocity (GHSV) of 9000 h<sup>-1</sup>. The reactor was loaded with 0.4 mL of catalyst (sieved to 125–250  $\mu$ m) between two beds of quartz wool. The catalysts were reduced prior to reaction under 20% H<sub>2</sub> in Ar at 300 °C (10 °C min<sup>-1</sup> ramp) and atmospheric pressure for 1 h. After reduction, a premixed feed of H<sub>2</sub> and CO<sub>2</sub> (3:1 molar ratio) was introduced to the reactor via mass flow controllers at 30 bar. Once the reaction reached steady state after 90 min, the product mixture was analyzed online by two gas chromatographs: one equipped with a thermal conductivity detector to quantify CO, CO2, and H<sub>2</sub> and one equipped with a flame ionization detector to quantify methanol, methane, and dimethyl ether. All product lines were heated above 100 °C to prevent product condensation.

# 3. RESULTS AND DISCUSSION

3.1. Structural and Compositional Characterization of Pd–In Alloys. Three different Pd–In/ $\gamma$ - $Al_2O_3$  alloy catalysts were prepared by employing the galvanic replacement (GR) method in which a controlled amount of palladium was exchanged with pre-reduced indium supported on  $\gamma$ - $Al_2O_3$ . The Pd concentration was varied to achieve distinct Pd surface structures with actual compositions of palladium and indium closely matching the nominal values, as confirmed by ICP-AES (Table S1). HAADF-STEM images, elemental mapping by

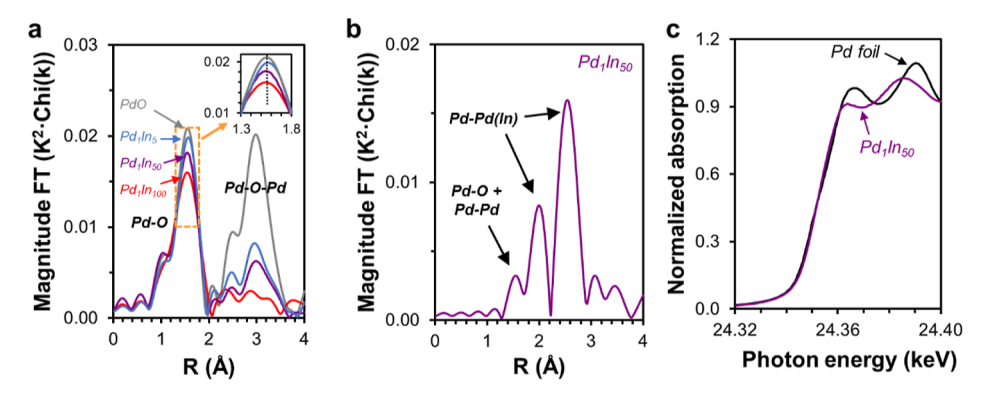


Figure 2. XAS of Pd–In alloys. (a) Ex situ Pd–K edge EXAFS spectra reference PdO (gray) and fresh Pd<sub>1</sub>In<sub>50</sub> (red), Pd<sub>1</sub>In<sub>50</sub> (purple), and Pd<sub>1</sub>In<sub>5</sub> (blue). Inset shows enlargement of the orange rectangular section. (b) In situ reduced Pd<sub>1</sub>In<sub>50</sub> (purple). (c) Pd K-edge XANES for in situ reduced Pd<sub>1</sub>In<sub>50</sub> (purple) and Pd foil reference (black).

EDS, and line scanning revealed that palladium was deposited on indium rather than the γ-Al<sub>2</sub>O<sub>3</sub> support and that Pd-In alloys were formed (Figures 1, S1-S3). In some cases, indium alone was detected (e.g., Pd<sub>1</sub>In<sub>100</sub>) due to the low palladium contents in the materials and the possibility of palladium being predominantly isolated (i.e., single atom alloy), which can be challenging to discern from the host metal. Representative spectra (from ~50 for each sample) for each catalyst are shown in Figure 1. Furthermore, the calculated d-spacing value of 0.229 nm (Figure S4) is similar to the value reported in the literature, which further supports alloy formation.<sup>16</sup> The average particle sizes of different fresh (prior to reaction) Pd-In alloys were estimated by STEM to be 2.5  $\pm$  1.6 nm for  $Pd_1In_5$  and 1.8  $\pm$  0.5 nm for  $Pd_1In_{50}$  Larger average particle sizes were observed after reaction, with Pd<sub>1</sub>In<sub>5</sub> increasing to 3.9  $\pm$  1.5 nm and Pd<sub>1</sub>In<sub>50</sub> increasing to 2.3  $\pm$  0.5 nm. Crystalline phase identification with XRD (Figure S5) proved challenging due to the small particle sizes (<5 nm) in the samples and the substantial overlaps between the reflections of the γ-Al<sub>2</sub>O<sub>3</sub> support oxide, Pd/Pd-In phases, and segregated In<sub>2</sub>O<sub>3</sub> particles. <sup>17,35</sup> However, a clear increase in the signal near 40°  $2\theta$  in the Pd<sub>1</sub>In<sub>5</sub> catalyst after reaction without any other clear changes is more consistent with the presence of a Pd-In alloy than pure Pd. Additionally, decreases in features at 21.7, 35.6, 51.2, and 60.8° corresponding to In<sub>2</sub>O<sub>3</sub> and In phases suggest that a larger fraction of the In is alloyed as the Pd content increases (Figure S5), a notion supported by the other techniques utilized here. XPS was used to assess the Pd/In ratios of the reduced fresh and spent catalysts (Figures S6 and S7, Table S2). Both surface and bulk atoms contribute substantially to the XPS data since the electron mean free path ( $\sim$ 1.5 nm) is comparable to the average particle radii ( $\sim$ 1–2 nm). Acknowledging that the technique is nonetheless biased toward the former, the tabulated data suggest that Pd<sub>1</sub>In<sub>50</sub> retains a substantially larger fraction of surface Pd after reaction than does Pd<sub>1</sub>In<sub>5</sub> (94 vs 58%). A larger fraction of Pd in Pd<sub>1</sub>In<sub>50</sub> may also be available for reaction than in Pd<sub>1</sub>In<sub>51</sub> leading to higher rates per Pd atom in the former.

**3.2. Coordination Environment via XAS.** XAS at the Pd K-edge was performed to evaluate the chemical bonding and electronic structure of these samples with in situ and ex situ studies. The  $k^2$ -weighted magnitudes of the Fourier transforms of the ex situ sample spectra in the EXAFS regime are displayed in Figure 2a. For the fresh samples, the XANES energy (23.2531 keV, Table S3) is characteristic of Pd<sup>2+</sup>. The EXAFS shows a first shell peak at a phase-uncorrected distance

of about 1.5 Å, attributed to Pd–O scattering. The fits of each sample indicate the presence of 4 Pd–O bonds at 2.05 Å, similar to the PdO reference. The higher shell peaks of the catalysts due to Pd–O–Pd scattering are much smaller than those in PdO, indicating the presence of small oxide clusters that decrease in size with decreasing Pd content. Dilution greatly impacts this feature, which becomes negligible for the sample with highest Pd dilution (Pd<sub>1</sub>In<sub>100</sub>). This suggests that Pd<sub>1</sub>In<sub>100</sub> alone may contain predominantly isolated Pd species. There is, therefore, likely a limiting concentration of Pd between 1:100 and 1:50 where sufficient Pd is present to enable aggregation.

The ex situ,  $k^2$ -magnitudes of the used catalysts (Figure S8) indicate that the majority of Pd is present in a metallic Pd or Pd-In alloy phase after reaction. In addition to the metallic peaks, there is a small fraction of oxidized Pd (i.e., peaks due to Pd-O) likely due to surface oxidation upon exposure to air. Since the atomic number of Pd and In differ by only 3, Pd-Pd and Pd-In configurations lead to almost identical scattering, making it impossible to resolve these two scattering paths. However, the metallic Pd-M bond distance is shifted toward slightly larger R for the Pd<sub>1</sub>In<sub>50</sub> and Pd<sub>1</sub>In<sub>5</sub> samples (inset of Figure 2a), indicating that strong interactions are present between Pd and In in these samples with different interatomic distances. $^{36-38}$  The Pd-M (M = Pd or In) coordination numbers (CN) in the used samples fall in the 4.6-5.7 range (Table S3), much smaller than that of bulk Pd (CN = 12), which suggests that much of the Pd is present at the surface of the nanoparticles. Pd-O CNs can additionally be used to assess the fraction of Pd at the surface by noting that surface Pd readily oxidizes in air to yield PdO with a Pd-O CN of 4; thus, dividing the measured Pd-O CN by 4 gives an estimation of the surface Pd content. 39,40 Pd<sub>1</sub>In<sub>100</sub> and Pd<sub>1</sub>In<sub>50</sub> materials have similar CNs of 1.3 (33% surface Pd) and 1.5 (38% surface Pd), respectively, whereas the CN of Pd<sub>1</sub>In<sub>5</sub> is substantially lower at 0.5 (13% surface Pd). The decrease in CN indicates that smaller portions of Pd atoms are located in the surface of Pd<sub>1</sub>In<sub>5</sub> compared to those observed in Pd<sub>1</sub>In<sub>100</sub> and Pd<sub>1</sub>In<sub>50</sub> materials. In the more diluted samples  $(Pd_1In_{100} \text{ and } Pd_1In_{50})$ , Pd atoms are kept in the surface due to stabilizing Pd-O interactions. This stabilization necessarily comes at the expense of similar In-O interactions; thus, a limit is reached with increasing Pd content above which additional Pd is preferentially found in the subsurface. Adsorbates present under reaction conditions are anticipated to cause similar stabilization phenomena. These data together suggest that

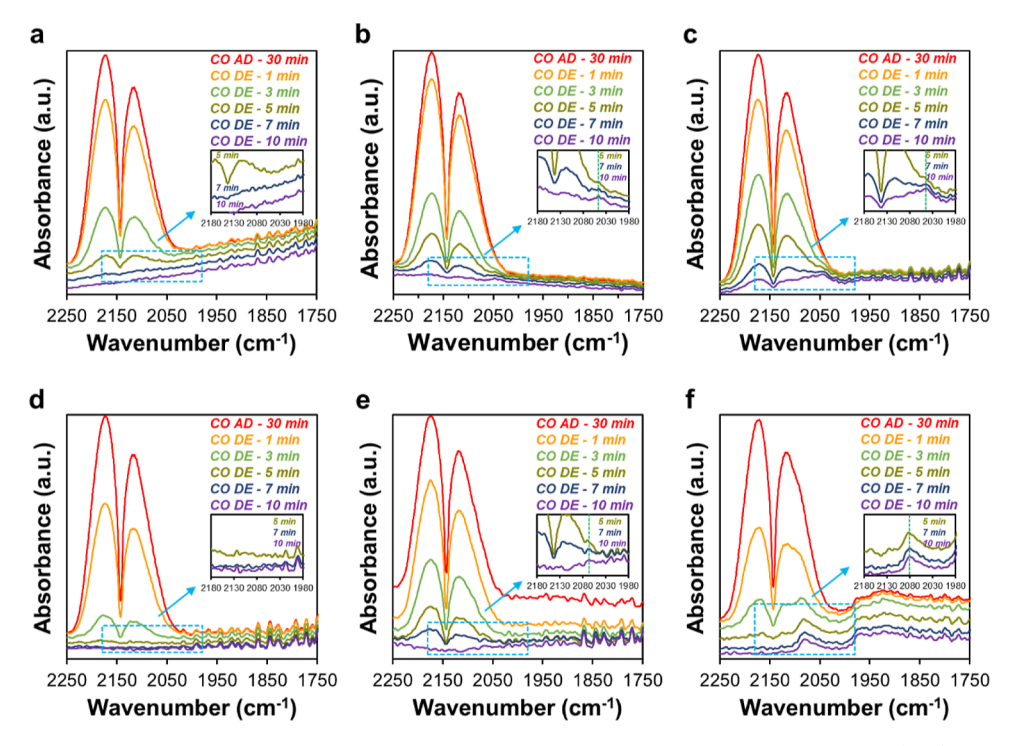


Figure 3. FTIR spectra of CO adsorbed at room temperature for Pd–In catalysts as a function of Pd loading. (a-c) Fresh reduced Pd<sub>1</sub>In<sub>100</sub>, Pd<sub>1</sub>In<sub>50</sub>, and Pd<sub>1</sub>In<sub>50</sub>, and Pd<sub>1</sub>In<sub>50</sub>, respectively. (d–f) Used Pd<sub>1</sub>In<sub>100</sub>, Pd<sub>1</sub>In<sub>50</sub>, and Pd<sub>1</sub>In<sub>5</sub>, respectively. The labels in the upper right corner indicate CO adsorption (CO AD) and CO desorption (CO DE) via He purge. Insets show enlarged sections of the corresponding rectangular sections.

increasing the Pd content from  $Pd_1In_{100}$  to  $Pd_1In_{50}$  primarily affects the aggregation of Pd but not its accessibility, while increasing Pd further to yield  $Pd_1In_5$  inefficiently incorporates Pd into the subsurface where it would be inaccessible for catalysis.

Upon reduction of Pd<sub>1</sub>In<sub>50</sub> (analyzed in situ), only metallic Pd-Pd/Pd-In scattering was observed (Figure 2b). This is consistent with the XANES spectra shown in Figure 2c. The XANES energies of these samples at the inflection of the leading edge are very similar to Pd foil (Table S3). The leading-edge intensity and white-line energy of Pd<sub>1</sub>In<sub>50</sub> differ substantially from those of Pd foil, however, which may indicate the presence of Pd-In neighbors (i.e., PdIn alloy formation). As discussed above, the Pd-Pd and Pd-In scattering paths are nearly identical, making deconvolution challenging. However, an average CN for the grouped Pd-Pd/ Pd-In interaction can be measured to be 7.4 (Table S3), consistent with nanoparticles in the 2-3 nm range. 41 At this size, one would expect a contraction of the bond distance if all interactions were derived from pure Pd. However, the average bond distance is larger than that of a Pd foil (2.77 vs 2.75 Å), consistent with the formation of a Pd-In alloy.

**3.3.** Ensemble Size Characterization via Infrared Spectroscopy of Adsorbed CO. The ensemble sizes of Pd in the alloy catalysts were further investigated by DRIFTS of adsorbed CO, which exhibits vibrational frequencies that are highly characteristic of the adsorption site. Figure 3 shows a series of DRIFT spectra in the 2250–1750 cm<sup>-1</sup> range for the fresh catalysts after reduction and after reaction (performed ex situ) without further treatment. These measurements were recorded at room temperature during CO exposure (adsorption) and a subsequent purge in He (desorption). The Pd<sub>1</sub>In<sub>100</sub> catalyst (Figure 3a) did not show any observable peaks for bound CO, suggesting that any Pd present in the alloy surface

is isolated since isolated Pd is known to adsorb CO much more weakly than pure Pd42 to the point that CO can fully desorb prior to the expulsion of gaseous CO from the DRIFTS cell. The absence of a clear peak for CO bound to isolated Pd atoms has also been noted in several prior studies. 17,43,44 This notion that Pd is predominantly isolated in this sample is additionally consistent with the EXAFS data. With a higher Pd loading, the Pd<sub>1</sub>In<sub>50</sub> catalyst showed a clear adsorption band at  $\sim$ 2050 cm<sup>-1</sup>, lower than the 2070–2110 cm<sup>-1</sup> region where CO typically adsorbs linearly atop Pd atoms. 45-49 This peak vanishes after 10 min of CO desorption, indicating weak binding to Pd relative to bulk Pd; thus, the Pd here must exist in a highly dispersed form such as sub-nanometer clusters. The lack of any observable peaks below 2000 cm<sup>-1</sup> corresponding to CO adsorbed to twofold and threefold Pd sites 46,50 provides further evidence that the Pd<sub>1</sub>In<sub>50</sub> catalyst does not contain substantial amounts of extended Pd ensembles (Figure 3b). The alloy with the highest Pd content (Pd<sub>1</sub>In<sub>5</sub>) similarly showed an adsorption band near 2050 cm<sup>-1</sup>, though it was much broader and quite persistent (remaining clearly visible after 20 min of CO desorption). No peak associated with bridge-bound CO was detected below 2000 cm<sup>-1</sup>. The increased persistence and breadth of the 2050 cm<sup>-1</sup> band is consistent with the Pd<sub>1</sub>In<sub>5</sub> alloy comprising ensembles that are larger on average and less uniform than those in Pd<sub>1</sub>In<sub>50</sub>, a notion also supported by STEM and EXAFS. In combination with the data discussed prior, these results allow for the three materials to be classified by their dominant states of Pd aggregation: isolated atoms for Pd<sub>1</sub>In<sub>100</sub>, small clusters for Pd<sub>1</sub>In<sub>50</sub>, and large clusters for Pd<sub>1</sub>In<sub>5</sub>.

This classification is further supported by CO DRIFT spectra of the post-reaction samples (Figure 3d-f). The  $Pd_1In_{100}$  catalyst does not show any new bands, suggesting that isolated Pd atoms do not aggregate under reaction conditions

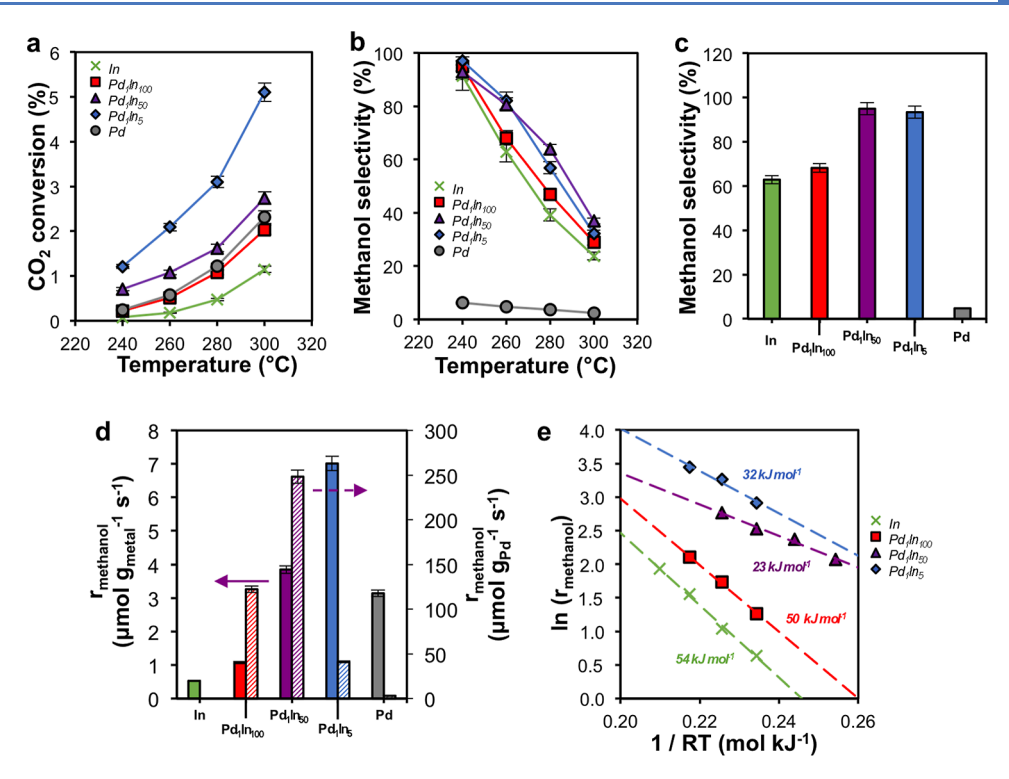


Figure 4. Catalytic performance of Pd–In alloy catalysts. (a) CO<sub>2</sub> conversion of Pd–In/Al<sub>2</sub>O<sub>3</sub> catalysts with different Pd loading at various reaction temperatures ( $H_2/CO_2 = 3:1$ , 30 bar, GHSV = 9000 h<sup>-1</sup>), compared to In/Al<sub>2</sub>O<sub>3</sub> and Pd/Al<sub>2</sub>O<sub>3</sub>. (b) Methanol selectivity for the aforementioned catalysts under similar reaction conditions as (a). (c) Methanol selectivity at 260 °C, 30 bar,  $H_2/CO_2 = 3:1$ , GHSV adjusted to obtain ~0.5% conversion for all catalysts. (d) Methanol synthesis rate per gram metal and per gram Pd at ~0.5% conversion. (e) Arrhenius plot (rate in units of  $\mu$ mol  $g_{catalyst}^{-1}$  min<sup>-1</sup>) and activation energies for the investigated catalysts. Subscripts indicate nominal molar ratios of metals. Pd<sub>1</sub>In<sub>100</sub> catalyst contains predominantly isolated Pd<sub>2</sub> Pd<sub>1</sub>In<sub>50</sub> contains small Pd clusters; and Pd<sub>1</sub>In<sub>5</sub> contains extended Pd ensembles.

when sufficiently diluted by In metal (Figure 3d). The Pd<sub>1</sub>In<sub>50</sub> catalyst does show some change after reaction, with a subtle blueshift in the CO IR peak at ~2050 cm<sup>-1</sup> by ~20 cm<sup>-1</sup> to  $\sim$ 2070 cm<sup>-1</sup>, which is consistent with the partial oxidation of Pd atoms in air. 51 As with the Pd<sub>1</sub>In<sub>50</sub> catalyst, no features below 2000 cm<sup>-1</sup> developed from the reaction, suggesting that these small Pd ensembles do not aggregate to form extended ensembles under reaction conditions. While a blueshift in the CO IR peak at ~2050 cm<sup>-1</sup> was also observed with the Pd<sub>1</sub>In<sub>5</sub> material, the most pronounced change was in the regime below 2000 cm<sup>-1</sup> where a broad feature appeared, indicating the presence of highly non-uniform bridge and hollow sites (Figure 3f). These bridge and hollow sites tend to bind CO strongly, as indicated by their persistence after extended desorption periods. These sites likely reside within larger clusters of Pd, which appear to be less resistant toward aggregation than smaller ensembles, a finding also noted by Pérez-Ramirez and co-workers with respect to their Pd/In<sub>2</sub>O<sub>3</sub> catalysts.<sup>17</sup>

**3.4.** Implications of Pd–In Alloy Surface Structure and Cluster Size on CO<sub>2</sub> Hydrogenation. To probe the effect of the different Pd ensemble sizes on CO<sub>2</sub> hydrogenation performance, the three alloys (Pd<sub>1</sub>In<sub>100</sub>, Pd<sub>1</sub>In<sub>50</sub>, and Pd<sub>1</sub>In<sub>5</sub> on Al<sub>2</sub>O<sub>3</sub>) along with In/Al<sub>2</sub>O<sub>3</sub> and Pd/Al<sub>2</sub>O<sub>3</sub> were tested for CO<sub>2</sub> hydrogenation to methanol. At the tested reaction temperatures (240–300 °C), all three Pd–In catalysts were stable for over 24 h (Figure S9), with methanol and CO comprising >80% of the analyzed products. At elevated temperatures (e.g., >260 °C), dimethyl ether and methane were also produced, accounting for the remaining products.

The addition of Pd to In was found to promote the reaction regardless of Pd loading. The CO<sub>2</sub> conversion increased from

0.2% with pure In to 0.5% with Pd<sub>1</sub>In<sub>100</sub> (isolated Pd), 1.1% with Pd<sub>1</sub>In<sub>50</sub> (small Pd clusters), and 2.1% with Pd<sub>1</sub>In<sub>5</sub> (large Pd clusters) at 260 °C (Figure 4a). In addition to improving the CO<sub>2</sub> conversion, the presence of Pd shifted the product distribution further toward methanol rather than CO, especially when Pd clusters were present. Pd<sub>1</sub>In<sub>50</sub> exhibited the highest methanol selectivity at 82%, while Pd<sub>1</sub>In<sub>5</sub> was similarly selective (80%) and Pd<sub>1</sub>In<sub>100</sub> was considerably less so (68%), although it was still more selective than pure In nanoparticles (62%) (Figure 4b). While Pd/Al<sub>2</sub>O<sub>3</sub>, on its own, was catalytically active for CO2 conversion under these conditions, it was significantly less selective to methanol, e.g., only 5% at 0.5% conversion. In addition to demonstrating the impact of Pd ensemble size on selectivity, this result also confirms that the galvanic replacement method was effective in depositing Pd exclusively on the In nanoparticles rather than the Al<sub>2</sub>O<sub>3</sub> support (which would have led to low methanol selectivities), in agreement with the STEM/EDS and XRD results.

These trends in methanol selectivity remain consistent when comparing the different catalytic materials at a fixed conversion of ~0.5% at 260 °C (Figure 4c). Under these conditions, the methanol selectivity increased upon addition of Pd to In from 62% for pure In to 68, 95, and 93% for Pd<sub>1</sub>In<sub>100</sub>, Pd<sub>1</sub>In<sub>50</sub>, and Pd<sub>1</sub>In<sub>5</sub>, respectively. These results are in line with prior literature discussing CO<sub>2</sub> hydrogenation over Pd supported on In<sub>2</sub>O<sub>3</sub> in which catalysts with predominantly isolated Pd yielded lower methanol selectivities than catalysts with clustered Pd. However, Pérez-Ramírez and co-workers also found that clusters of more than two Pd atoms began to behave more like metallic Pd, compromising methanol

production. A similar deleterious behavior was not observed in the present study, as no significant decline in the methanol selectivity was detected between Pd<sub>1</sub>In<sub>50</sub> and Pd<sub>1</sub>In<sub>5</sub>. Our results demonstrate that aggregated Pd within In, even at the relatively high loadings present in Pd<sub>1</sub>In<sub>5</sub>, remains selective to methanol, whereas Pd clusters on In<sub>2</sub>O<sub>3</sub> do not. Notably, the Pd/In<sub>2</sub>O<sub>3</sub> catalysts in that study contained similar Pd/In ratios to those used here (1:101 for 0.75 wt % Pd on In<sub>2</sub>O<sub>3</sub>), ruling out a substantial compositional difference causing the discrepancy in behavior. This result reveals an important distinction between the catalytic performance of Pd sites in metal-on-oxide single (or few) atom catalysts and the metal-inmetal alloys present in the series of materials examined in the present study. Indeed, the synthesis approach utilized here allowed for the manipulation of Pd loading and structure to a greater extent than the prior Pd/In<sub>2</sub>O<sub>3</sub> materials (which relied on conventional synthesis methods such as dry impregnation and coprecipitation) while maintaining high methanol selectivity and abating CO formation.

Examining the methanol synthesis rate as a function of metal content reveals that Pd is most efficiently utilized when in small clusters. Normalizing rates to the total metal loading (Pd + In) shows pure In nanoparticles to be the least catalytically active and  $Pd_1In_5$  to be the most (Figure 4d), but the improvement in the methanol synthesis rate from  $Pd_1In_5$  to  $Pd_1In_{50}$  does not scale with Pd content. As a result, the Pd-specific rate (i.e., the rate per mass of Pd) for  $Pd_1In_{50}$  is 2 times that of  $Pd_1In_{100}$ , 6 times that of  $Pd_1In_5$ , and 80 times that of pure Pd. This suggests that the large clusters in the  $Pd_1In_5$  catalyst are less catalytically active than the small clusters in  $Pd_1In_{50}$ .

The different dependencies of rate on temperature for the In-based materials further support our hypothesis that distinct active sites comprising different Pd ensemble sizes give rise to the different catalytic performances of each catalyst (Figure 4e). The activation energy on pure In  $(54 \pm 2 \text{ kJ mol}^{-1})$  is similar to that of Pd<sub>1</sub>In<sub>100</sub>  $(50 \pm 2 \text{ kJ mol}^{-1})$  while substantially higher than that of Pd<sub>1</sub>In<sub>50</sub>  $(23 \pm 2 \text{ kJ mol}^{-1})$ , which is just below that of Pd<sub>1</sub>In<sub>5</sub>  $(32 \pm 6 \text{ kJ mol}^{-1})$ . These activation energy differences suggest that the active sites themselves change with dilution, especially when comparing Pd<sub>1</sub>In<sub>50</sub> and Pd<sub>1</sub>In<sub>5</sub> to Pd<sub>1</sub>In<sub>100</sub>. The non-monotonic relationship between the apparent activation energy and Pd content further highlights the important point that Pd ensembles larger than an atom but smaller than those in bulk Pd nanoparticles are the most efficient active sites for the CO<sub>2</sub> hydrogenation reaction.

Together, these data suggest that the most effective spatial arrangement of Pd atoms in Pd-In alloys for CO<sub>2</sub> hydrogenation into methanol is a small cluster. As the Pd content increases from Pd<sub>1</sub>In<sub>100</sub> to Pd<sub>1</sub>In<sub>50</sub>, specific rates and selectivities increase due to the presence of these clusters. As the Pd content further increases from  $Pd_1In_{50}$  to  $Pd_1In_{5}$ , the Pd is less efficiently used due to the trapping of Pd beneath the surface and possibly within aggregates. These trends fit with a mechanistic picture where Pd aggregates are responsible for promoting H<sub>2</sub> activation, while the Pd-In interface is responsible for hydrogenation itself. Similar rate promotions for aggregated vs isolated atoms of Pd have been noted in prior works with Au, Ag, and Ga hosts. While isolated Pd in Au is capable of dissociating H<sub>2</sub>, the resulting H atoms are not strongly stabilized because they interact very weakly with Au. 55-57 Clusters of Pd provide bridge and hollow sites where H atoms can be strongly stabilized via coordination with

multiple Pd atoms. Friend and co-workers showed how this shifts the rate-limiting step in H<sub>2</sub>/D<sub>2</sub> exchange from dissociation (of H<sub>2</sub> or D<sub>2</sub>) to re-association (of H with D) and increases the overall reaction rate.<sup>58</sup> While the subsequent spillover step from Pd to Au does not appear to be rate-limiting to H<sub>2</sub>/D<sub>2</sub> exchange, its endothermic nature has raised questions about the ability of the dissociated hydrogen to participate substantially in catalytic reactions on these materials. This is thought to be the case in PdAg catalysts as well, as noted by Greiner and co-workers with regard to acetylene hydrogenation.<sup>59</sup> In this case, increasing the Pd content is necessary to bring Pd atoms sufficiently close together for the H2 dissociated on one Pd atom to be accessible to acetylene bound to another. Electronic factors also play an important role in these materials, especially in the PdGa intermetallics prepared from high-temperature melts investigated by Armbrüster and co-workers. 60 In these structures, the Pd atoms are formally isolated from one another in both PdGa and Pd2Ga stoichiometries, though the latter material contains Pd atoms in closer proximity (2.8 vs 3.0 Å shortest Pd-Pd distance) and has a d-band with a substantially higher density of states at the Fermi level (0.3 vs 0.1 states eV<sup>-1</sup> atom<sup>-1</sup>). These changes underly an increase in acetylene hydrogenation rate for Pd2Ga vs PdGa by a factor of 30. A Pd<sub>2</sub>In intermetallic produced in the same manner showed comparable catalytic behavior due to similarities in electronic structure, though the dilution effect was not critiqued for this material. The decrease in Pd-specific rate for Pd<sub>1</sub>In<sub>5</sub> (large clusters) vs Pd<sub>1</sub>In<sub>50</sub> (small clusters) can be explained by (1) the more extensive partitioning of Pd into the inaccessible bulk and (2) the lower fraction of surface Pd atoms which are adjacent to In atoms. The importance of the Pd-In interface in selective CO<sub>2</sub> hydrogenation to methanol has been noted both theoretically and experimentally. In studies of Pd/In<sub>2</sub>O<sub>3</sub> models by Ge and co-workers, the interfacial Pd-In sites of 4-atom and 13-atom Pd clusters were found to be selective for methanol formation and possess similar reactivities.<sup>52</sup> Snider et al. supported these findings, experimentally showing that the adjacency of Pd and In atoms in Pd-In intermetallic alloys are the active site for CO<sub>2</sub> hydrogenation to methanol, operating synergistically with the In<sub>2</sub>O<sub>3</sub> support.<sup>53</sup> Similarly, Armbrüster and co-workers further found In<sub>x</sub>Pd<sub>y</sub> intermetallics supported on In<sub>2</sub>O<sub>3</sub> to be 99% selective to CO<sub>2</sub> in methanol steam reforming.<sup>54</sup> Isotopic labeling experiments further suggested that the active site is linked to the interface of InPd/In2O3. Therefore, smaller Pd clusters yield higher rates per Pd atom since a larger fraction of the Pd within them is present at this interface. Coincidentally, the high Pd loadings used to produce these lead to Pd being trapped beneath the surface and therefore being inaccessible for catalysis.

#### 4. CONCLUSIONS

Pd–In alloys with distinct atomic configurations were synthesized via galvanic replacement and utilized to promote the selective hydrogenation of CO<sub>2</sub> to methanol. Obtaining definitive conclusions regarding atomic ensembles in dilute alloys from any one characterization method presents a major challenge due to the low signals these materials typically yield; thus, we probed Pd–In alloy structures here using a multipronged approach. The synthesis method employed enabled the production of alloys with distinct Pd ensembles that yielded stable catalytic performance in this reaction. Our

findings further lead us to conclude that Pd can be most efficiently used to promote selective CO<sub>2</sub> hydrogenation to methanol (up to 95% selectivity) when present in small clusters, while isolated Pd is both less reactive and selective and large clusters of Pd inefficiently trap Pd below the nanoparticle surface or in the interior of Pd islands, away from reactive Pd—In interfaces. Developing further understanding of how to manipulate galvanic replacement to generate unique reactive structures in dilute alloys on under-researched host metals, such as In, and examining how these materials behave with less "innocent" supports will expand the toolkit that catalysis researchers have to address sustainability challenges in synthesizing the chemicals that underpin the global economy.

## ASSOCIATED CONTENT

## Supporting Information

The Supporting Information is available free of charge at https://pubs.acs.org/doi/10.1021/acscatal.3c01861.

Additional characterizations (HRTEM, STEM, EDX mapping image, XRD patterns, XPS, and XAS), stability test, ICP, and XAS fitting data (PDF)

# AUTHOR INFORMATION

#### **Corresponding Author**

Nathaniel M. Eagan — Department of Chemical and Biological Engineering, Tufts University, Medford, Massachusetts 02155, United States; orcid.org/0000-0002-0219-8941; Email: nathaniel.eagan@tufts.edu

#### **Authors**

Abdulaziz M. Alamer – Chemical and Biomolecular Engineering, University of California, Los Angeles, Los Angeles, California 90095, United States; Department of Chemical and Biological Engineering, Tufts University, Medford, Massachusetts 02155, United States

Mengyao Ouyang — Department of Chemical and Biological Engineering, Tufts University, Medford, Massachusetts 02155, United States

Faisal H. Alshafei — Chemical and Biomolecular Engineering, University of California, Los Angeles, Los Angeles, California 90095, United States; Division of Chemistry and Chemical Engineering, California Institute of Technology, Pasadena, California 91125, United States; orcid.org/0000-0003-1808-1374

Muhammad Amtiaz Nadeem – Surface Science and Advanced Characterization, Corporate Research and Development (CRD), Saudi Basic Industries Corporation (SABIC) at KAUST, Thuwal 23955, Saudi Arabia

Yahya Alsalik — Surface Science and Advanced Characterization, Corporate Research and Development (CRD), Saudi Basic Industries Corporation (SABIC) at KAUST, Thuwal 23955, Saudi Arabia; orcid.org/0000-0001-5690-0938

Jeffrey T. Miller — Davidson School of Chemical Engineering, Purdue University, West Lafayette, Indiana 47907, United States; oorcid.org/0000-0002-6269-0620

Maria Flytzani-Stephanopoulos – Department of Chemical and Biological Engineering, Tufts University, Medford, Massachusetts 02155, United States

E. Charles H. Sykes – Department of Chemistry, Tufts University, Medford, Massachusetts 02155, United States; orcid.org/0000-0002-0224-2084 Vasilios Manousiouthakis — Chemical and Biomolecular Engineering, University of California, Los Angeles, Los Angeles, California 90095, United States; orcid.org/ 0000-0003-1548-0097

Complete contact information is available at: https://pubs.acs.org/10.1021/acscatal.3c01861

#### **Author Contributions**

The manuscript was written through contributions of all authors. All authors have given approval to the final version of the manuscript.

#### **Funding**

This work was financially supported by Saudi Basic Industries Corporation. J.T.M. was partially funded by the National Science Foundation under Cooperative Agreement No. EEC-1647722. The XAS experiments of this research used beamline 8-ID (ISS) of the National Synchrotron Light Source II, a U.S. Department of Energy (DOE) Office of Science User Facility operated for the DOE Office of Science by Brookhaven National Laboratory under contract no. DE-SC0012704. E.C.H.S. thanks the DOE/BES Catalysis Science Program for support under grant #DE-SC0021196. N.M.E thanks Integrated Mesoscale Architectures for Sustainable Catalysis (IMASC), an Energy Frontier Research Center funded by the U.S. Department of Energy, Office of Science, Basic Energy Sciences supported under award #DE-SC0012573.

#### Notes

The authors declare no competing financial interest.

## ACKNOWLEDGMENTS

Authors acknowledge Dr. Eli Stavitski for assistance with XAS data collection and Georgios Giannakakis for assistance in XAS data collection as well as useful conversations regarding interpretations of various data. A.M.A. acknowledges Sabic T&I for sponsoring his graduate studies. F.H.A. acknowledges Aramco R&D for funding his graduate studies.

## REFERENCES

- (1) Climate Change 2021: The Physical Science Basis. In Contribution of Working Group I to the Sixth Assessment Report of the Intergovernmental Panel on Climate Change; Masson-Delmotte, V., Zhai, P., Pirani, A., Connors, S. L., Péan, C., Berger, S., Caud, N., Chen, Y., Goldfarb, L., Gomis, M. I., Huang, M., Leitzell, K., Lonnoy, E., Matthews, J. B. R., Maycock, T. K., Waterfield, T., Yelekçi, Ö., Yu, R., Zhou, B., Eds.; Cambridge University Press, 2021; pp 1–2391.
- (2) Monastersky, R. Global Carbon Dioxide Levels near Worrisome Milestone. *Nature* **2013**, 497, 13–14.
- (3) Wang, W.; Wang, S.; Ma, X.; Gong, J. Recent Advances in Catalytic Hydrogenation of Carbon Dioxide. *Chem. Soc. Rev.* **2011**, 40, 3703.
- (4) Navarro-Jaén, S.; Virginie, M.; Bonin, J.; Robert, M.; Wojcieszak, R.; Khodakov, A. Y. Highlights and Challenges in the Selective Reduction of Carbon Dioxide to Methanol. *Nat. Rev. Chem.* **2021**, *5*, 564–579.
- (5) English, A.; Brown E&C, J.; Rovner, J.; Davies, S. Methanol. In *Kirk-Othmer Encyclopedia of Chemical Technology*; American Cancer Society, 2015; pp 1–19.
- (6) Qian, Q.; Zhang, J.; Cui, M.; Han, B. Synthesis of Acetic Acid via Methanol Hydrocarboxylation with CO2 and H2. *Nat. Commun.* **2016**, *7*, 11481.
- (7) Somiari, I.; Manousiouthakis, V. Coproduction of Acetic Acid and Hydrogen/Power from Natural Gas with Zero Carbon Dioxide Emissions. *AIChE J.* **2018**, *64*, 860–876.

- (8) Waters, T.; O'Hair, R. A. J.; Wedd, A. G. Catalytic Gas Phase Oxidation of Methanol to Formaldehyde. *J. Am. Chem. Soc.* **2003**, *125*, 3384–3396.
- (9) Xu, M.; Lunsford, J. H.; Goodman, D. W.; Bhattacharyya, A. Synthesis of Dimethyl Ether (DME) from Methanol over Solid-Acid Catalysts. *Appl. Catal., A* **1997**, *149*, 289–301.
- (10) Olah, G. A. Beyond Oil and Gas: The Methanol Economy. *Angew. Chem., Int. Ed.* **2005**, 44, 2636–2639.
- (11) Behrens, M.; Studt, F.; Kasatkin, I.; Kühl, S.; Hävecker, M.; Abild-Pedersen, F.; Zander, S.; Girgsdies, F.; Kurr, P.; Kniep, B.-L.; Tovar, M.; Fischer, R. W.; Nørskov, J. K.; Schlögl, R. The Active Site of Methanol Synthesis over Cu/ZnO/Al2O3 Industrial Catalysts. *Science* 2012, 336, 893–897.
- (12) Fichtl, M. B.; Schlereth, D.; Jacobsen, N.; Kasatkin, I.; Schumann, J.; Behrens, M.; Schlögl, R.; Hinrichsen, O. Kinetics of Deactivation on Cu/ZnO/Al2O3 Methanol Synthesis Catalysts. *Appl. Catal., A* **2015**, 502, 262–270.
- (13) Ye, J.; Liu, C.; Ge, Q. DFT Study of CO2 Adsorption and Hydrogenation on the In2O3 Surface. *J. Phys. Chem. C* **2012**, *116*, 7817–7825.
- (14) Ye, J.; Liu, C.; Mei, D.; Ge, Q. Active Oxygen Vacancy Site for Methanol Synthesis from CO2 Hydrogenation on In2O3(110): A DFT Study. ACS Catal. 2013, 3, 1296–1306.
- (15) Martin, O.; Martín, A. J.; Mondelli, C.; Mitchell, S.; Segawa, T. F.; Hauert, R.; Drouilly, C.; Curulla-Ferré, D.; Pérez-Ramírez, J. Indium Oxide as a Superior Catalyst for Methanol Synthesis by CO <sub>2</sub> Hydrogenation. *Angew. Chem.* **2016**, *128*, 6369–6373.
- (16) Rui, N.; Wang, Z.; Sun, K.; Ye, J.; Ge, Q.; Liu, C. CO2 Hydrogenation to Methanol over Pd/In2O3: Effects of Pd and Oxygen Vacancy. *Appl. Catal.*, B **2017**, 218, 488–497.
- (17) Frei, M. S.; Mondelli, C.; García-Muelas, R.; Kley, K. S.; Puértolas, B.; López, N.; Safonova, O. V.; Stewart, J. A.; Curulla Ferré, D.; Pérez-Ramírez, J. Atomic-Scale Engineering of Indium Oxide Promotion by Palladium for Methanol Production via CO2 Hydrogenation. *Nat. Commun.* **2019**, *10*, 3377.
- (18) Han, Z.; Tang, C.; Wang, J.; Li, L.; Li, C. Atomically Dispersed Ptn+ Species as Highly Active Sites in Pt/In2O3 Catalysts for Methanol Synthesis from CO2 Hydrogenation. *J. Catal.* **2021**, 394, 236–244.
- (19) Sun, K.; Rui, N.; Zhang, Z.; Sun, Z.; Ge, Q.; Liu, C.-J. A Highly Active Pt/In <sub>2</sub> O <sub>3</sub> Catalyst for CO <sub>2</sub> Hydrogenation to Methanol with Enhanced Stability. *Green Chem.* **2020**, 22, 5059–5066.
- (20) Therrien, A. J.; Hensley, A. J. R.; Marcinkowski, M. D.; Zhang, R.; Lucci, F. R.; Coughlin, B.; Schilling, A. C.; McEwen, J.-S.; Sykes, E. C. H. An Atomic-Scale View of Single-Site Pt Catalysis for Low-Temperature CO Oxidation. *Nat. Catal.* **2018**, *1*, 192–198.
- (21) Wang, H.; Liu, J.-X.; Allard, L. F.; Lee, S.; Liu, J.; Li, H.; Wang, J.; Wang, J.; Oh, S. H.; Li, W.; Flytzani-Stephanopoulos, M.; Shen, M.; Goldsmith, B. R.; Yang, M. Surpassing the Single-Atom Catalytic Activity Limit through Paired Pt-O-Pt Ensemble Built from Isolated Pt1 Atoms. *Nat. Commun.* **2019**, *10*, 3808.
- (22) Zhang, X.; Cui, G.; Feng, H.; Chen, L.; Wang, H.; Wang, B.; Zhang, X.; Zheng, L.; Hong, S.; Wei, M. Platinum—Copper Single Atom Alloy Catalysts with High Performance towards Glycerol Hydrogenolysis. *Nat. Commun.* **2019**, *10*, 5812.
- (23) Marcinkowski, M. D.; Darby, M. T.; Liu, J.; Wimble, J. M.; Lucci, F. R.; Lee, S.; Michaelides, A.; Flytzani-Stephanopoulos, M.; Stamatakis, M.; Sykes, E. C. H. Pt/Cu Single-Atom Alloys as Coke-Resistant Catalysts for Efficient C–H Activation. *Nat. Chem.* **2018**, 10, 325–332.
- (24) Jeong, H.; Lee, G.; Kim, B.-S.; Bae, J.; Han, J. W.; Lee, H. Fully Dispersed Rh Ensemble Catalyst To Enhance Low-Temperature Activity. J. Am. Chem. Soc. 2018, 140, 9558–9565.
- (25) Kliewer, C. J.; Aliaga, C.; Bieri, M.; Huang, W.; Tsung, C.-K.; Wood, J. B.; Komvopoulos, K.; Somorjai, G. A. Furan Hydrogenation over Pt(111) and Pt(100) Single-Crystal Surfaces and Pt Nanoparticles from 1 to 7 Nm: A Kinetic and Sum Frequency Generation Vibrational Spectroscopy Study. *J. Am. Chem. Soc.* **2010**, *132*, 13088–13095.

- (26) Shan, J.; Liu, J.; Li, M.; Lustig, S.; Lee, S.; Flytzani-Stephanopoulos, M. NiCu Single Atom Alloys Catalyze the CH Bond Activation in the Selective Non-Oxidative Ethanol Dehydrogenation Reaction. *Appl. Catal., B* **2018**, 226, 534–543.
- (27) Giannakakis, G.; Trimpalis, A.; Shan, J.; Qi, Z.; Cao, S.; Liu, J.; Ye, J.; Biener, J.; Flytzani-Stephanopoulos, M. NiAu Single Atom Alloys for the Non-Oxidative Dehydrogenation of Ethanol to Acetaldehyde and Hydrogen. *Top. Catal.* **2018**, *61*, 475–486.
- (28) Zhang, M.; Yang, B.; Yu, Y. A Density Functional Theory Study on the Conversion of Ethylene to Carbon Monomer on PdAu(100) Surface. *Appl. Surf. Sci.* **2015**, *356*, 1252–1261.
- (29) Lucci, F. R.; Liu, J.; Marcinkowski, M. D.; Yang, M.; Allard, L. F.; Flytzani-Stephanopoulos, M.; Sykes, E. C. H. Selective Hydrogenation of 1,3-Butadiene on Platinum—Copper Alloys at the Single-Atom Limit. *Nat. Commun.* **2015**, *6*, 8550.
- (30) Boucher, M. B.; Zugic, B.; Cladaras, G.; Kammert, J.; Marcinkowski, M. D.; Lawton, T. J.; Sykes, E. C. H.; Flytzani-Stephanopoulos, M. Single Atom Alloy Surface Analogs in Pd0.18Cu15 Nanoparticles for Selective Hydrogenation Reactions. *Phys. Chem. Chem. Phys.* **2013**, *15*, 12187–12196.
- (31) Miyazaki, M.; Furukawa, S.; Takayama, T.; Yamazoe, S.; Komatsu, T. Surface Modification of PdZn Nanoparticles via Galvanic Replacement for the Selective Hydrogenation of Terminal Alkynes. *ACS Appl. Nano Mater.* **2019**, *2*, 3307–3314.
- (32) Xia, X.; Wang, Y.; Ruditskiy, A.; Xia, Y. 25th Anniversary Article: Galvanic Replacement: A Simple and Versatile Route to Hollow Nanostructures with Tunable and Well-Controlled Properties. *Adv. Mater.* **2013**, *25*, 6313–6333.
- (33) Lu, X.; Chen, J.; Skrabalak, S. E.; Xia, Y. Galvanic Replacement Reaction: A Simple and Powerful Route to Hollow and Porous Metal Nanostructures. *Proc. Inst. Mech. Eng., Part N: J. Nanoeng. Nanosyst.* **2007**, 221, 1–16.
- (34) Men, Y.; Kolb, G.; Zapf, R.; O'Connell, M.; Ziogas, A. Methanol Steam Reforming over Bimetallic Pd–In/Al2O3 Catalysts in a Microstructured Reactor. *Appl. Catal., A* **2010**, 380, 15–20.
- (35) Cao, Y.; Sui, Z.; Zhu, Y.; Zhou, X.; Chen, D. Selective Hydrogenation of Acetylene over Pd-In/Al <sub>2</sub> O <sub>3</sub> Catalyst: Promotional Effect of Indium and Composition-Dependent Performance. *ACS Catal.* **2017**, *7*, 7835–7846.
- (36) Feng, Q.; Zhao, S.; Wang, Y.; Dong, J.; Chen, W.; He, D.; Wang, D.; Yang, J.; Zhu, Y.; Zhu, H.; Gu, L.; Li, Z.; Liu, Y.; Yu, R.; Li, J.; Li, Y. Isolated Single-Atom Pd Sites in Intermetallic Nanostructures: High Catalytic Selectivity for Semihydrogenation of Alkynes. *J. Am. Chem. Soc.* **2017**, *139*, 7294–7301.
- (37) Li, C.; Chen, Y.; Zhang, S.; Xu, S.; Zhou, J.; Wang, F.; Wei, M.; Evans, D. G.; Duan, X. Ni–In Intermetallic Nanocrystals as Efficient Catalysts toward Unsaturated Aldehydes Hydrogenation. *Chem. Mater.* **2013**, 25, 3888–3896.
- (38) Li, C.; Chen, Y.; Zhang, S.; Zhou, J.; Wang, F.; He, S.; Wei, M.; Evans, D. G.; Duan, X. Nickel-Gallium Intermetallic Nanocrystal Catalysts in the Semihydrogenation of Phenylacetylene. *ChemCatChem* **2014**, *6*, 824–831.
- (39) Fang, Y.-L.; Miller, J. T.; Guo, N.; Heck, K. N.; Alvarez, P. J. J.; Wong, M. S. Structural Analysis of Palladium-Decorated Gold Nanoparticles as Colloidal Bimetallic Catalysts. *Catal. Today* **2011**, *160*, 96–102.
- (40) Zhao, Z.; Miller, J. T.; Wu, T.; Schweitzer, N. M.; Wong, M. S. EXAFS Characterization of Palladium-on-Gold Catalysts Before and After Glycerol Oxidation. *Top. Catal.* **2015**, *58*, 302–313.
- (41) Miller, J. T.; Kropf, A. J.; Zha, Y.; Regalbuto, J. R.; Delannoy, L.; Louis, C.; Bus, E.; van Bokhoven, J. A. The Effect of Gold Particle Size on AuAu Bond Length and Reactivity toward Oxygen in Supported Catalysts. *J. Catal.* **2006**, 240, 222–234.
- (42) Darby, M. T.; Sykes, E. C. H.; Michaelides, A.; Stamatakis, M. Carbon Monoxide Poisoning Resistance and Structural Stability of Single Atom Alloys. *Top. Catal.* **2018**, *61*, 428–438.
- (43) Abbet, S.; Riedo, E.; Brune, H.; Heiz, U.; Ferrari, A. M.; Giordano, L.; Pacchioni, G. Identification of Defect Sites on

- MgO(100) Thin Films by Decoration with Pd Atoms and Studying CO Adsorption Properties. *J. Am. Chem. Soc.* **2001**, *123*, 6172–6178. (44) Liu, J.; Shan, J.; Lucci, R.; Cao, S.; Sykes, E. C. H.; Flytzani-Stephanopoulos, M. Palladium—Gold Single Atom Alloy Catalysts for Liquid Phase Selective Hydrogenation of 1-Hexyne. *Catal. Sci. Technol.* **2017**, *7*, 4276–4284.
- (45) Luneau, M.; Shirman, T.; Filie, A.; Timoshenko, J.; Chen, W.; Trimpalis, A.; Flytzani-Stephanopoulos, M.; Kaxiras, E.; Frenkel, A. I.; Aizenberg, J.; Friend, C. M.; Madix, R. J. Dilute Pd/Au Alloy Nanoparticles Embedded in Colloid-Templated Porous SiO 2: Stable Au-Based Oxidation Catalysts. *Chem. Mater.* **2019**, *31*, 5759–5768.
- (46) Jeon, J.; Kon, K.; Toyao, T.; Shimizu, K.; Furukawa, S. Design of Pd-Based Pseudo-Binary Alloy Catalysts for Highly Active and Selective NO Reduction. *Chem. Sci.* **2019**, *10*, 4148–4162.
- (47) Wu, Z.; Wegener, E. C.; Tseng, H.-T.; Gallagher, J. R.; Harris, J. W.; Diaz, R. E.; Ren, Y.; Ribeiro, F. H.; Miller, J. T. Pd-In Intermetallic Alloy Nanoparticles: Highly Selective Ethane Dehydrogenation Catalysts. *Catal. Sci. Technol.* **2016**, *6*, 6965–6976.
- (48) Markov, P. V.; Bukhtiyarov, A. V.; Mashkovsky, I. S.; Smirnova, N. S.; Prosvirin, I. P.; Vinokurov, Z. S.; Panafidin, M. A.; Baeva, G. N.; Zubavichus, Ya. V.; Bukhtiyarov, V. I.; Stakheev, A. Yu. PdIn/Al2O3 Intermetallic Catalyst: Structure and Catalytic Characteristics in Selective Hydrogenation of Acetylene. *Kinet. Catal.* **2019**, *60*, 842–850.
- (49) Markov, P. V.; Smirnova, N. S.; Baeva, G. N.; Bukhtiyarov, A. V.; Mashkovsky, I. S.; Stakheev, A. Yu. Intermetallic Pd In /Al2O3 Catalysts with Isolated Single-Atom Pd Sites for One-Pot Hydrogenation of Diphenylacetylene into Trans-Stilbene. *Mendeleev Commun.* 2020, 30, 468–471.
- (50) Ouyang, M.; Papanikolaou, K. G.; Boubnov, A.; Hoffman, A. S.; Giannakakis, G.; Bare, S. R.; Stamatakis, M.; Flytzani-Stephanopoulos, M.; Sykes, E. C. H. Directing Reaction Pathways via in Situ Control of Active Site Geometries in PdAu Single-Atom Alloy Catalysts. *Nat. Commun.* **2021**, *12*, 1549.
- (51) Zorn, K.; Giorgio, S.; Halwax, E.; Henry, C. R.; Grönbeck, H.; Rupprechter, G. CO Oxidation on Technological Pd–Al2O3 Catalysts: Oxidation State and Activity. *J. Phys. Chem. C* **2011**, *115*, 1103–1111.
- (52) Ye, J.; Liu, C.; Mei, D.; Ge, Q. Methanol Synthesis from CO2 Hydrogenation over a Pd4/In2O3 Model Catalyst: A Combined DFT and Kinetic Study. *J. Catal.* **2014**, *317*, 44–53.
- (53) Snider, J. L.; Streibel, V.; Hubert, M. A.; Choksi, T. S.; Valle, E.; Upham, D. C.; Schumann, J.; Duyar, M. S.; Gallo, A.; Abild-Pedersen, F.; Jaramillo, T. F. Revealing the Synergy between Oxide and Alloy Phases on the Performance of Bimetallic In–Pd Catalysts for CO <sub>2</sub> Hydrogenation to Methanol. *ACS Catal.* **2019**, *9*, 3399–3412.
- (54) Köwitsch, N.; Thoni, L.; Klemmed, B.; Benad, A.; Paciok, P.; Heggen, M.; Köwitsch, I.; Mehring, M.; Eychmüller, A.; Armbrüster, M. Proving a Paradigm in Methanol Steam Reforming: Catalytically Highly Selective In  $_{\rm x}$  Pd  $_{\rm y}$  /In  $_{\rm 2}$  O  $_{\rm 3}$  Interfaces. ACS Catal. 2021, 11, 304–312.
- (55) Hammer, B.; Norskov, J. K. Why Gold Is the Noblest of All the Metals. *Nature* **1995**, *376*, 238–240.
- (56) Lucci, F. R.; Darby, M. T.; Mattera, M. F. G.; Ivimey, C. J.; Therrien, A. J.; Michaelides, A.; Stamatakis, M.; Sykes, E. C. H. Controlling Hydrogen Activation, Spillover, and Desorption with Pd–Au Single-Atom Alloys. *J. Phys. Chem. Lett.* **2016**, *7*, 480–485.
- (57) Tierney, H. L.; Baber, A. E.; Kitchin, J. R.; Sykes, E. C. H. Hydrogen Dissociation and Spillover on Individual Isolated Palladium Atoms. *Phys. Rev. Lett.* **2009**, *103*, 246102.
- (58) van der Hoeven, J. E. S.; Ngan, H. T.; Taylor, A.; Eagan, N. M.; Aizenberg, J.; Sautet, P.; Madix, R. J.; Friend, C. M. Entropic Control of HD Exchange Rates over Dilute Pd-in-Au Alloy Nanoparticle Catalysts. ACS Catal. 2021, 11, 6971–6981.
- (59) Hartwig, C.; Schweinar, K.; Jones, T. E.; Beeg, S.; Schmidt, F.-P.; Schlögl, R.; Greiner, M. Isolated Pd Atoms in a Silver Matrix: Spectroscopic and Chemical Properties. *J. Chem. Phys.* **2021**, *154*, 184703.

(60) Luo, Y.; Alarcón Villaseca, S.; Friedrich, M.; Teschner, D.; Knop-Gericke, A.; Armbrüster, M. Addressing Electronic Effects in the Semi-Hydrogenation of Ethyne by InPd2 and Intermetallic Ga–Pd Compounds. *J. Catal.* **2016**, 338, 265–272.